PERGAMON

International Journal of Solids and Structures 40 (2003) 3537–3556

INTERNATIONAL JOURNAL OF SOLIDS and STRUCTURES

www.elsevier.com/locate/ijsolstr

Contact forces in anisotropic frictional granular materials

N.P. Kruyt *

Department of Mechanical Engineering, University of Twente, P.O. Box 217, 7500 AE Enschede, The Netherlands

Received 24 June 2002; received in revised form 17 February 2003

Abstract

The probability density functions (PDFs) of contact forces in anisotropic, cohesionless and frictional granular materials are studied numerically and theoretically. Using discrete element simulations of biaxial deformation of a large two-dimensional assembly consisting of 200,000 disks, it is observed that the PDFs for the normal and tangential components of the contact forces depend significantly on contact orientation. The PDFs exhibit exponential decay and the PDF for the tangential component of the contact forces is not always symmetrical with respect to zero tangential force. The shape of the PDF for the normal component of the contact forces changes with shear strain. A qualitative explanation for this change is given that is related to the biaxial deformation mechanism in which the disrupted contacts are predominantly oriented in the direction of the minor principle stress.

A maximum entropy method is employed to study these PDFs theoretically, using a prescribed stress tensor as constraint. It is found that the theoretical results correspond qualitatively to many of the results obtained from the discrete element simulations. Discrepancies between theory and simulations are attributed to the fact that the kinematics have not been taken into account in the theory.

Keywords: Granular materials; Force probability density function; Maximum entropy method; Anisotropy

1. Introduction

Recently, there has been considerable interest in the probabilistic characteristics of contact forces in granular materials in quasi-static equilibrium. These characteristics are important in obtaining a more profound understanding of the behaviour of granular materials. Furthermore, this knowledge may be of more practical interest, such as in probabilistic continuum-mechanical models of failure and fracture. In a probabilistic framework the contact forces are described by the probability density function (PDF for short). Such PDFs have been studied experimentally, theoretically and numerically.

The experimental studies by Mueth et al. (1998), Løvoll et al. (1999), Makse et al. (2000) and Blair et al. (2001) show that in isotropic assemblies the PDF for the normal component of the contact forces generally

* Tel.: +31-53-489-2528; fax: +31-53-489-3695.
E-mail address: n.p.kruyt@utwente.nl (N.P. Kruyt).

0020-7683/03/$ - see front matter © 2003 Elsevier Science Ltd. All rights reserved.
doi:10.1016/S0020-7683(03)00148-3

exhibits exponential decay. However, for high pressures Makse et al. (2000) observed a Gaussian-type PDF.

Theoretical studies of PDFs for contact forces generally employ two types of methods, lattice-type methods and maximum entropy methods. Lattice-type methods were developed by Coppersmith et al. (1996), Socolar (1998) and Nguyen and Coppersmith (2000). They assume a probabilistic propagation of contact forces that does not seem to reflect the statically indeterminate, structure-like nature of granular materials where elastic effects are significant. An important result of the lattice model by Coppersmith et al. (1996) is that the exponential decay of the PDF for the normal component of the contact forces can be predicted theoretically. A maximum entropy method for quasi-static deformation of granular materials was first proposed by Rothenburg (1980). It was subsequently used by Bagi (1997) and Kruyt and Rothenburg (2002b) to study the PDF for the contact forces. Bagi (1997) showed that the PDF exhibits exponential decay, while Kruyt and Rothenburg (2002b) obtained the PDFs for the normal and tangential components of the contact forces for isotropic assemblies. These PDFs demonstrate the importance of dry Coulomb friction for cohesionless granular materials.

Numerous numerical studies of the PDFs for the contact forces have been performed, for example by Radjaï et al. (1996), Thornton (1997), Thornton and Antony (1998), Makse et al. (2000), Antony (2000) and Kruyt and Rothenburg (2002b). These studies generally use the discrete element method, as proposed by Cundall and Strack (1979). Such discrete element simulations are very suitable in micromechanical studies, since they can provide results which cannot be obtained easily by direct measurements, such as forces at internal contacts and tangential forces in particular. The PDFs obtained from these simulations show qualitative agreement with those obtained experimentally. Quantitative differences between the results of the various simulations may be due to the different parameters used, such as packing density, stress level and the contact constitutive relation.

The previous studies mostly focused on the PDF for the normal component of the contact forces in isotropic assemblies. The emphasis of this study will be on PDFs for the normal *and* the tangential component of the contact forces in anisotropic assemblies. To this end two-dimensional discrete element simulations are performed of biaxial deformation of a large assembly of 200,000 disks. The biaxial deformation results in induced anisotropy of the assembly (Rothenburg and Bathurst, 1989). The PDFs for the contact forces are also studied theoretically, using a maximum entropy method.

The outline of this study is as follows. In Section 2 the various micromechanical quantities are defined and the micromechanical expression for the average stress tensor is given. In Section 3 the discrete element simulations are described, including the contact constitutive relation that was used. In Section 4 the PDFs are given for the normal and tangential components of the contact forces, as determined from the discrete element simulations. Section 5 deals with the theoretical study of the PDF for the contact forces, using a maximum entropy method. Finally, findings from this study are discussed.

The usual sign convention from soil mechanics is employed here, which means that compressive stresses and strains are considered positive. Furthermore, the summation convention is used, by which a summation is implied over repeated subscripts.

2. Micromechanics

Micromechanics of quasi-static deformation of granular materials deals with the study between microscopic characteristics and macroscopic characteristics. For assemblies of semi-rigid particles the microscopic level is that of *contacts*, where the quantities of interest are force and relative displacement between particles. The macroscopic quantities of interest are the average stress and strain tensors. An important objective of micromechanics is to formulate macroscopic constitutive relations in terms of microscopic

quantities, such as the contact constitutive relation that relates the force and the relative displacement at the contact.

The force at the contact that is exerted by particle q on particle p is denoted by f_i^{pq}. In the two-dimensional case considered here the relative displacement Δ_i^{pq} between particles in contact is defined by

$$\Delta_i^{pq} = [U_i^q + e_{ji}\omega^q r_j^{qp}] - [U_i^p + e_{ji}\omega^p r_j^{pq}] \tag{1}$$

where U_i^p is the displacement of the centre of particle p, ω^p is its rotation, e_{ij} is the two-dimensional permutation tensor and r_i^{pq} is the vector from the centre of particle p to the point of contact between particles p and q, see also Fig. 1. Also shown in Fig. 1 are the unit normal vector n_i^{pq}, the unit tangential vector t_i^{pq} at the contact point and the branch vector l_i^{pq}. The branch vector is the vector connecting the centres of the particles that are in contact. The orientation of a contact is denoted by θ^{pq}, such that $n_i^{pq} = \{\cos\theta^{pq}, \sin\theta^{pq}\}^{\mathrm{T}}$.

The primary statistical quantities describing the contact geometry of the assembly of particles are coordination number Γ and the contact distribution function $S(\theta)$. Coordination number is the average number of contacts per particle. For isotropic assemblies it is a measure of the packing density of the assembly, see Kruyt and Rothenburg (1996). The contact distribution function (Horne, 1965) is defined such that $S(\theta)\,\Delta\theta$ is the fraction of contacts with orientation θ in the interval $(\theta, \theta + \Delta\theta)$. An example of an anisotropic contact distribution function, as determined from results of a discrete element simulation, is shown in Fig. 2.

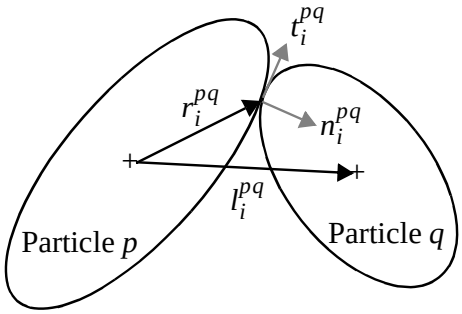

Fig. 1. Geometrical quantities associated with two particles in contact.

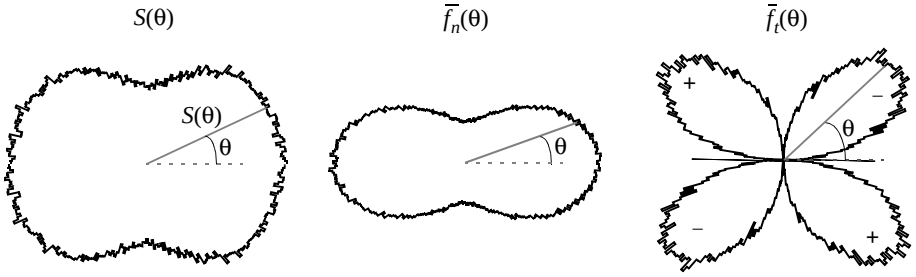

Fig. 2. Polar plots of the contact distribution function and the group averages of normal and tangential contact forces.

The most important macroscopic quantities are the stress tensor σ_{ij} and the strain tensor ε_{ij}. The micromechanical expression for the average stress tensor in terms of contact forces f_i^c and branch vectors l_i^c is (see for example, Drescher and de Josselin de Jong, 1972; Strack and Cundall, 1978; Rothenburg and Selvadurai, 1981; Mehrabadi et al., 1982)

$$\sigma_{ij} = \frac{1}{A} \sum_{c \in C} f_i^c l_j^c \tag{2}$$

where the summation is over the contacts c in the set C in the region of interest with area A.

From continuum-mechanical considerations it is expected that points that are separated by a vector $l_i = \{l\cos\theta, l\sin\theta\}^{\mathrm{T}}$ show a relative displacement $\varepsilon_{ij} l_j$. This means that the relative displacement depends on orientation θ. Therefore it is logical to group contacts with similar orientations and to analyse *group averages* for relative displacements and forces at contacts (Rothenburg and Bathurst, 1989; Bathurst and Rothenburg, 1990). The group averages for the normal and tangential forces are denoted by $\bar{f}_{\mathrm{n}}(\theta)$ and $\bar{f}_{\mathrm{t}}(\theta)$, respectively. Polar plots of such group averages, as determined from results of a discrete element simulation, are shown in Fig. 2.

For analytical manipulations it is advantageous to transform a sum over contacts of a generic contact quantity ϕ^c to an integral form. Using the definitions of the contact distribution function $S(\theta)$ and the group average $\bar{\phi}(\theta)$, this transformation is established by

$$\frac{1}{A} \sum_{c \in C} \phi^c = m_{\mathrm{A}} \int_0^{2\pi} S(\theta) \bar{\phi}(\theta) \, \mathrm{d}\theta \tag{3}$$

where m_{A} is the contact density, i.e. the number of contacts per area.

Fig. 2 shows that the group averages of the contact forces, and hence the statistical characteristics in general, depend significantly on contact orientation θ. For a complete description of the probabilistic characteristics of the contact forces it is therefore necessary to consider the *conditional* PDF $P_f(\boldsymbol{f}|\theta)$ of the contact force given the contact orientation θ.

The group average $\bar{\phi}(\theta)$ of a generic contact quantity ϕ^c is determined from the PDF $P_f(\boldsymbol{f}|\theta)$ by

$$\bar{\phi}(\theta) = \int_f \phi(\boldsymbol{f}, \theta) P_f(\boldsymbol{f}|\theta) \, \mathrm{d}\boldsymbol{f} \tag{4}$$

Since $P_f(\boldsymbol{f}|\theta)$ is a PDF, it must satisfy the normalising condition

$$\bar{1}(\theta) = 1 \tag{5}$$

The overall average $\langle\phi\rangle$ is finally defined by integrating the group average over all contact orientations θ

$$\langle\phi\rangle = \int_0^{2\pi} S(\theta) \bar{\phi}(\theta) \, \mathrm{d}\theta \tag{6}$$

Using this notation, the micromechanical expression (2) for the stress tensor becomes

$$\sigma_{ij} = m_{\mathrm{A}} \langle f_i l_j \rangle \tag{7}$$

3. Discrete element simulations

In this section the contact constitutive relation is described that is used in the discrete element simulations. The basic characteristics of the initial assembly are also given, and the biaxial deformation that is imposed on this assembly is described. The evolution with shear strain of the macroscopic shear strength

and volumetric strain are shown, as well as that of coordination number and contact anisotropy that together describe the primary statistics of the contact geometry.

3.1. Contact constitutive relation and initial assembly

The contact constitutive relation used in the discrete element simulations is basically that employed by Cundall and Strack (1979). It involves elastic and Coulomb frictional effects. The elastic component of the constitutive relation is described by two linear springs in the normal and tangential direction at the contact with spring constants k_n and k_t, respectively. Hence, the normal component f_n^c and the tangential component f_t^c of the contact force are related to the normal component Δ_n^c and the tangential component Δ_t^c of the relative displacement at the contact by

$$f_n^c = k_n \Delta_n^c \qquad f_t^c = k_t \Delta_t^c \tag{8}$$

with the restriction that only compressive normal forces are allowed. If the normal force were to become negative, the contact is considered to be broken for cohesionless materials. Furthermore, the tangential force is limited by Coulomb friction, i.e. $|f_t^c| \leqslant \mu f_n^c$ where μ is the friction coefficient. The range of admissible contact forces is shown in Fig. 3.

The initial, isotropic assembly consists of 200,000 disks from a fairly wide, lognormal particle-size distribution with average particle radius R_{avg}. The initial packing density, i.e. the total area occupied by the particles divided by the area of the assembly, is $\nu = 0.850$. The initial coordination number is $\Gamma = 4.07$. The hydrostatic confining stress σ is such that $\sigma/(k_n R_{avg}) = 5 \times 10^{-3}$ and the stiffness ratio $k_t/k_n = 0.5$. The friction coefficient μ that is mainly considered is $\mu = 0.5$, while $\mu = 0.1$ and 0.3 are used in some additional simulations.

The procedure employed to create the fairly dense, isotropic initial assembly consists of four steps. The first step involves the determination of random initial positions for the disks such that there are no contacts. In the second step this extremely loose assembly is slowly compacted with zero friction coefficient μ until the prescribed hydrostatic confining stress σ is obtained. In the third step the assembly is isotropically expanded by 1%, leading to a reduction in confining stress σ. In the fourth step, the assembly is once again compressed isotropically with the friction coefficient μ set to the lowest value considered ($\mu = 0.1$) until the prescribed hydrostatic confining stress σ is obtained. These last two steps in the creation of the initial assembly are performed in order to allow tangential forces to develop.

The case considered here is that without body forces acting on the particles, since the presence of body forces would lead to a heterogeneous average stress field.

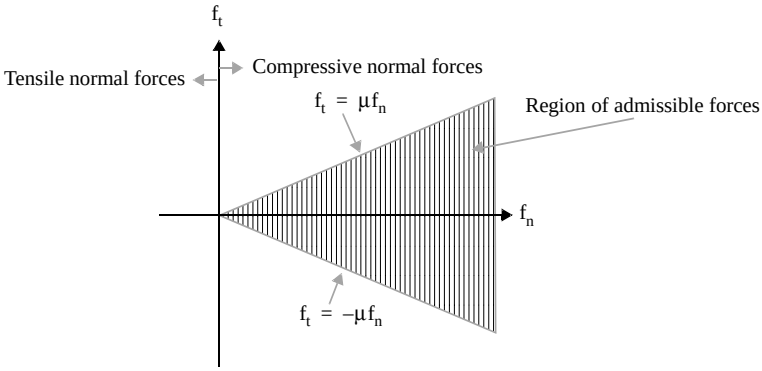

Fig. 3. Region of admissible contact forces.

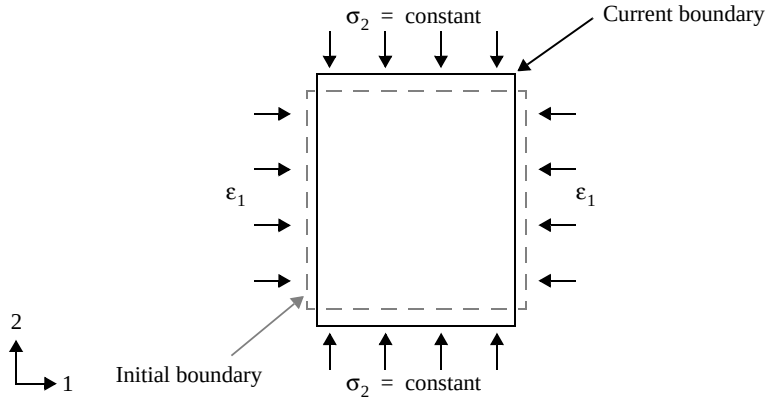

Fig. 4. Schematic of biaxial deformation.

3.2. Biaxial deformation, macroscopic behaviour and group averages

The isotropic initial assembly is subjected to biaxial deformation, as sketched in Fig. 4. A compressive (principal) strain ε_1 is imposed in the horizontal direction, while the (principal) stress σ_2 in the vertical direction is kept constant. For this type of deformation σ_1 in the horizontal direction will be the major principle stress, while σ_2 in the vertical direction will be the minor principle stress. Pressure p, shear stress q, volumetric strain ε_V and shear strain ε_S are then defined by

$$\begin{aligned} p &= \tfrac{1}{2}(\sigma_1 + \sigma_2) \qquad q = \tfrac{1}{2}(\sigma_1 - \sigma_2) \\ \varepsilon_V &= \varepsilon_1 + \varepsilon_2 \qquad \varepsilon_S = \varepsilon_1 - \varepsilon_2 \end{aligned} \tag{9}$$

The maximum strain ε_1 that was applied in the simulations is $\varepsilon_1 = 0.10$. The simulations were performed using periodic boundaries (Cundall, 1986) in order to minimize boundary effects.

The macroscopic shear strength q/p and the volumetric strain ε_V that are observed from the simulation are shown in Fig. 5. The shear strength increases from zero in the initial isotropic state to a peak strength, and then gradually decreases. For small strains the volumetric strain corresponds to (elastic) compression of the material, while for larger strains the material dilates. This type of behaviour is characteristic for granular materials in a fairly dense initial packing.

From the simulations the contact distribution function $S(\theta)$ and the group averages of the normal forces $\bar{f}_n(\theta)$ and of the tangential forces $\bar{f}_t(\theta)$ could be determined, see Fig. 2 for an example.

The results can be represented by Fourier series (Rothenburg and Bathurst, 1989; Bathurst and Rothenburg, 1990)

$$S(\theta) \cong \frac{1}{2\pi}[1 + a_c \cos 2(\theta - \theta_0)] \tag{10}$$

$$\bar{f}_n(\theta) \cong f_0[1 + a_n \cos 2(\theta - \theta_0)] \qquad \bar{f}_t(\theta) \cong -f_0 a_t \sin 2(\theta - \theta_0) \tag{11}$$

Here θ_0 is the direction of the major principle stress ($\theta_0 = 0°$ for the configuration shown in Fig. 4), which is assumed to coincide with the direction of contact anisotropy. Parameter a_c describes the anisotropy of the contact distribution function $S(\theta)$. Parameter f_0 is a measure of the average normal force, a_n is a measure of the anisotropy in the distribution of the normal forces and a_t is a measure of the magnitude of the tangential forces, relative to the normal forces.

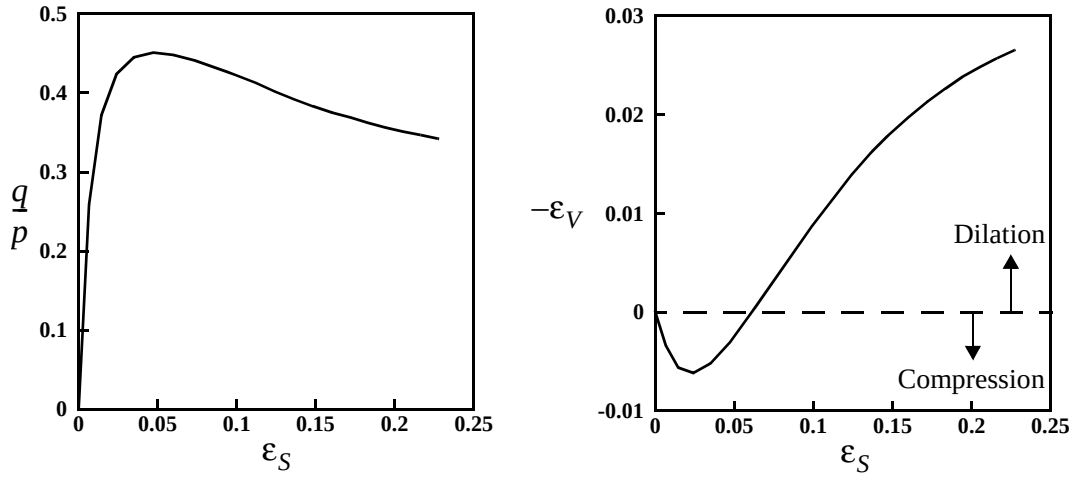

Fig. 5. Evolution with shear strain ε_S of shear strength q/p and volumetric strain ε_V for discrete element simulation with friction coefficient $\mu = 0.5$.

As was shown by Rothenburg and Bathurst (1989), see also Bathurst and Rothenburg (1990), the parameters a_c, a_n and a_t are related to the shear strength q/p by the stress–force–fabric relation

$$\frac{q}{p} \cong \frac{1}{2}[a_c + a_n + a_t] \tag{12}$$

Since the strains correspond to compression in the horizontal direction and to extension in the vertical direction, it is expected that the contacts that are broken during the biaxial deformation are predominantly oriented in the vertical direction. This is manifested by changes in coordination number Γ and contact anisotropy a_c, see Fig. 6. Coordination number Γ gradually decreases until it reaches an approximately constant value. Contact anisotropy a_c increases from zero in the initial isotropic state until it reaches a

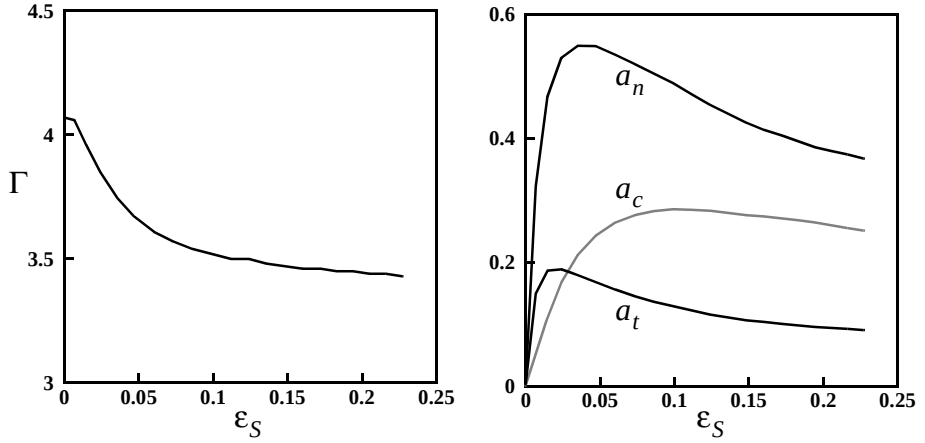

Fig. 6. Evolution with shear strain ε_S of coordination number Γ and parameters a_c, a_n and a_t for discrete element simulation with friction coefficient $\mu = 0.5$.

peak, and then gradually decreases. Note that the strains corresponding to peak strength q/p and peak anisotropy a_c do not coincide. The other parameters a_n and a_t show a behaviour that is similar to that of a_c.

4. Probability density functions of contact forces

Since the assembly consists of 200,000 particles, it is possible to determine the conditional PDFs for the contact forces (given the contact orientation θ) with reasonable accuracy. The marginal PDFs for the normal and tangential forces are denoted by $P_n(f_n|\theta)$ and $P_t(f_t|\theta)$, respectively. To determine these for a fixed contact orientation θ, all contacts whose orientation is in an interval with a width of 10° around this value were used as data to estimate the PDFs. Histograms of these were determined by dividing the ranges of contact forces into 50 bins.

The PDFs for the contact forces are conveniently shown in terms of the nondimensional normal force ξ and the nondimensional tangential force η. These are defined by

$$\begin{aligned} \xi &= \frac{f_n}{\bar{f}_n} \quad \xi \geqslant 0 \\ \eta &= \frac{f_t}{\mu \bar{f}_n} \quad -\infty < \eta < \infty \end{aligned} \tag{13}$$

The parameter $\rho(\theta)$, relating group averages of normal and tangential forces, is defined by

$$\rho(\theta) = \frac{\bar{f}_t(\theta)}{\mu \bar{f}_n(\theta)} \tag{14}$$

and hence $-1 < \rho(\theta) < 1$.

Results for the PDFs $P_\xi(\xi|\theta)$ for the nondimensional force ξ and $P_\eta(\eta|\theta)$ for the nondimensional tangential force η are shown for the initial isotropic assembly ($\varepsilon_S = 0.0$), for the state corresponding to peak strength ($\varepsilon_S = 0.047$) and for the state corresponding to large strain ($\varepsilon_S = 0.227$). For the initial isotropic state $P_\xi(\xi|\theta)$ and $P_\eta(\eta|\theta)$ are independent of θ. For the states corresponding to peak strength and large strain, the PDFs have been determined for contact orientations $\theta = 0°$, $\theta = 45°$ and $\theta = 90°$.

The PDFs in the initial isotropic state are shown in Fig. 7. The PDF P_ξ for the normal forces does not equal zero for $\xi = 0$. The PDF P_η for the tangential forces is symmetrical around $\eta = 0$ and it is rather narrow. These PDFs closely resemble those given by Kruyt and Rothenburg (2002b), although quantitative differences are present in the PDF P_η for the tangential force. These are caused by the differences in packing density and confining stress.

The PDFs for the states that correspond to peak strength and to large strain are shown in Fig. 8. The PDFs at peak strength are shown in black, while the PDFs at large strain are shown in grey. Except for $\theta = 0°$, the PDFs at peak strength and at large strain are very similar. The PDFs for $\theta = 0°$ are qualitatively the same as those in the initial isotropic state. The PDFs P_ξ for the normal forces at $\theta = 45°$ and $\theta = 90°$ are qualitatively different from that in the initial state. The probability density at $\xi = 0$ has increased. For $\theta = 0°$ and $\theta = 45°$ the peak of the PDF P_ξ is found at ξ between 0.5 and 1.0, while for $\theta = 90°$ the peak of the PDF is found at $\xi = 0$. In comparison with the initial isotropic state, the PDFs P_η for the tangential forces are much wider. For $\theta = 45°$ the PDF P_η is no longer symmetrical around $\eta = 0$.

Parameter ρ, as defined in (14), equals zero for $\theta = 0°$ and $\theta = 90°$. For $\theta = 45°$, we have $\rho = -0.35$ at peak strength and $\rho = -0.18$ at large strain.

For large forces ($\xi \gg 1$ and $|\eta| \gg 1$) the PDFs exhibit exponential decay, i.e.

$$\ln P_\xi \cong -r_\xi \xi + C_\xi \qquad \ln P_\eta \cong -r_\eta |\eta| + C_\eta \tag{15}$$

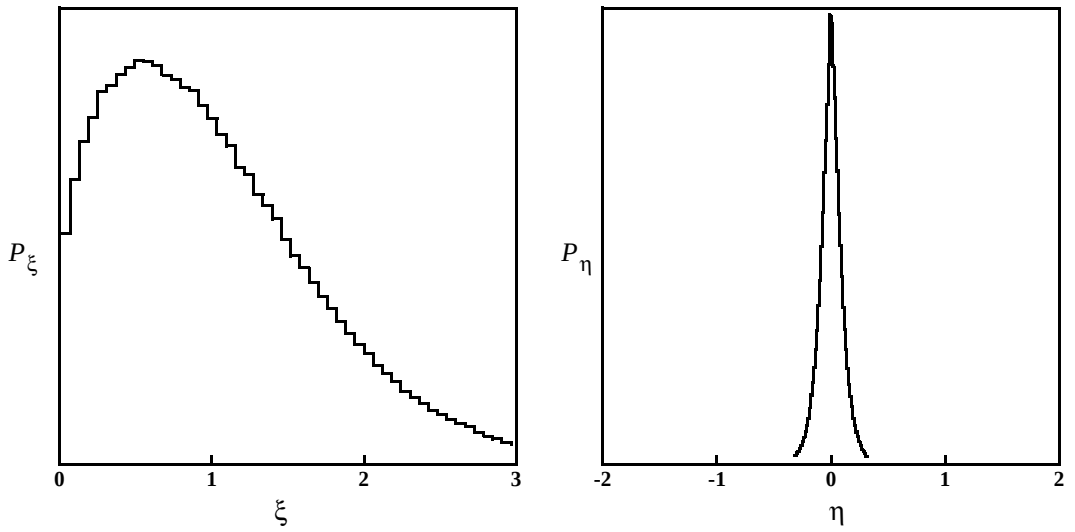

Fig. 7. PDFs for the nondimensional normal and tangential forces for the initial isotropic assembly. Results from discrete element simulation with $\mu = 0.5$.

where r_ξ and r_η are the decay rates. For the isotropic state this exponential decay was shown experimentally by Mueth et al. (1998) and Løvoll et al. (1999), while Radjaï et al. (1996) and Kruyt and Rothenburg (2002b) observed this from simulations. Fig. 9 for the PDFs at peak strength and $\theta = 45°$ shows that exponential decay of the contact forces also occurs in anisotropic assemblies. Here the decay rates are $r_\xi \cong 2.8$, $r_\eta \cong 3.2$ for negative η and $r_\eta = 4.6$ for positive η.

The most notable differences between the PDF P_η for the tangential forces in the initial isotropic state and the other anisotropic states are that in the anisotropic states it is much wider and that it no longer is symmetrical around $\eta = 0$ for $\theta = 45°$. The PDFs are wider in the anisotropic states due to the biaxial deformation mechanism which leads to greatly increased relative displacements between particles, and hence to a far wider range of tangential forces. For $\theta = 45°$ the PDF is asymmetrical since the group average tangential force $\bar{f}_t$ is not zero for $\theta = 45°$, see Fig. 2. Fig. 2 also shows that for $\theta = 0°$ and $\theta = 90°$ (where PDFs are symmetrical around $\eta = 0$), $\bar{f}_t$ equals zero.

A notable difference between the PDFs P_ξ in the initial isotropic state and the other anisotropic states is that for the anisotropic states at $\theta = 0°$ the peak in the PDF is found at larger nondimensional force. In addition, in the anisotropic states the peak in the PDF P_ξ is found at $\xi = 0$ for $\theta = 90°$.

These trends can be explained by considering the biaxial deformation mechanism and the associated loss of contacts in the vertical direction of the minor principle stress $\theta = 90°$. It follows from (10) with $\theta_0 = 0°$ that the number of contacts in the horizontal direction of the major principle stress $\theta = 0°$ is characterized by $\Gamma(1 + a_c)$, while that in the vertical direction $\theta = 90°$ is characterized by $\Gamma(1 - a_c)$. The evolution with shear strain ε_S of these quantities is shown in Fig. 10. Indeed the number of contacts in the horizontal direction with compressive strain mildly increases, while the number of contacts in the vertical direction with extensile strain strongly decreases. Similarly, it follows from (11) that the average normal force in the horizontal direction is given by $f_0(1 + a_n)$, while that in the vertical direction is given by $f_0(1 - a_n)$. Fig. 10 shows that the average normal force in the horizontal direction increases strongly, while in the vertical direction it is approximately constant. For $\theta = 90°$, many contacts will be broken. In general, the contacts that tend to be broken are the contacts that have a relatively small normal force. Hence, in the PDF P_ξ these contacts will be located before the peak in the PDF for the isotropic state. Therefore the observations that

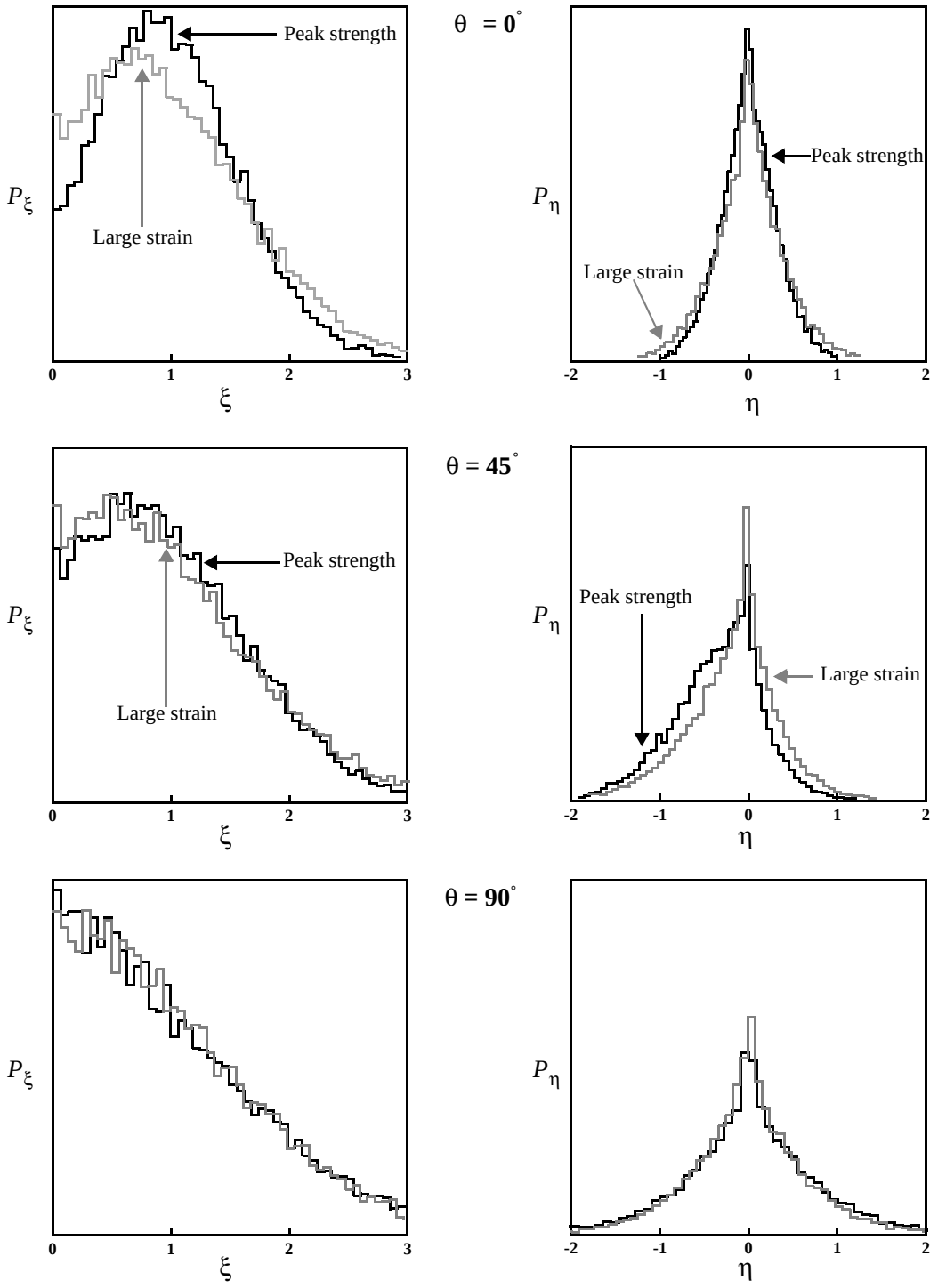

Fig. 8. PDFs for the nondimensional normal and tangential forces at peak strength (in black) and at large strain (in grey). Results from discrete element simulation with friction coefficient $\mu = 0.5$.

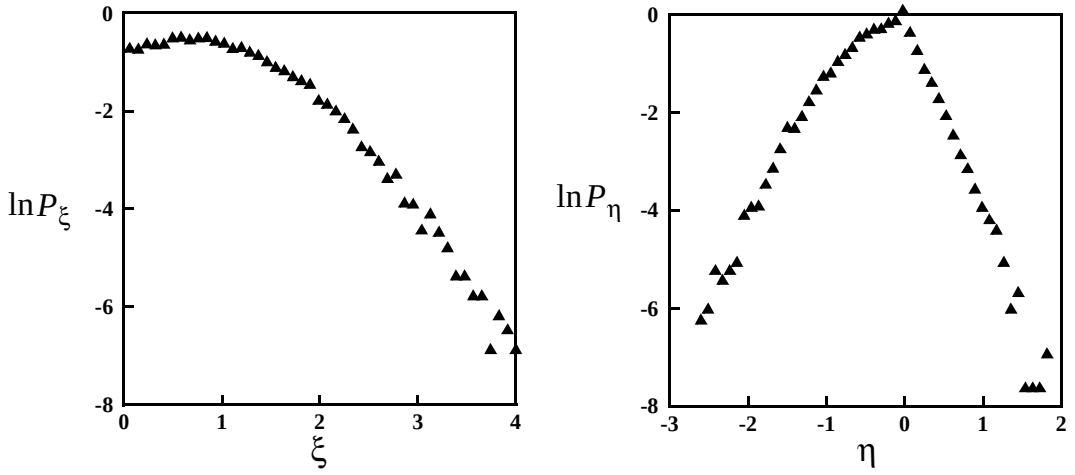

Fig. 9. Plot of the logarithm of the PDFs for the nondimensional normal and tangential forces, showing exponential decay. Results from discrete element simulation with friction coefficient $\mu = 0.5$, corresponding to the state at peak strength and $\theta = 45°$.

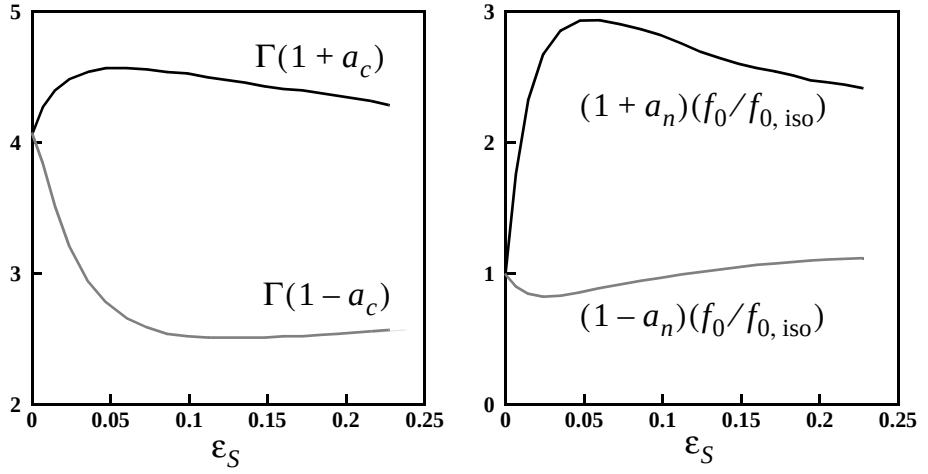

Fig. 10. Evolution with shear strain ε_S of the number of contacts in horizontal and vertical directions and of the average normal force in horizontal and vertical directions, relative to the isotropic initial state. Results from discrete element simulation with friction coefficient $\mu = 0.5$.

the average normal force is constant combined with the decrease of the number of contacts provide a qualitative explanation of the change of the PDF P_ξ from that found in the isotropic state, see Fig. 7, to that shown in Fig. 8 for the anisotropic states for $\theta = 90°$.

This process of loss of contacts for $\theta = 90°$ at small strains is shown in another way in Fig. 11. This gives the number of contacts (not the probability density) with certain normal forces (not nondimensional force) for three values of shear strain ε_S just before the strain corresponding to peak strength. Clearly noticeable is the reduction in the number of contacts, especially for low normal forces. Also evident in Fig. 11 is the increase in the average normal force for $\theta = 0°$.

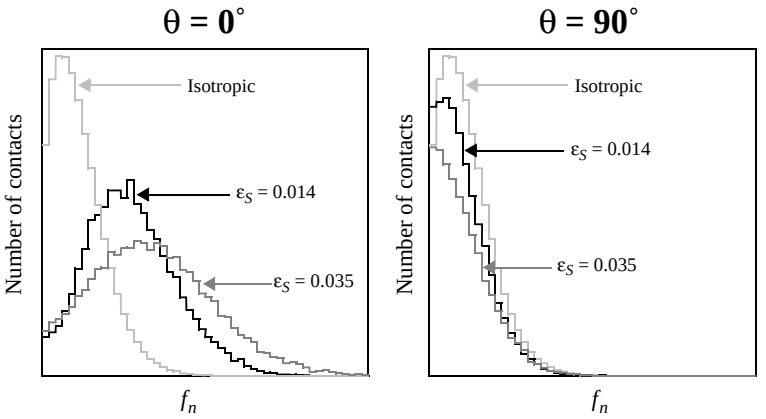

Fig. 11. Change in number of contacts with certain normal forces. Results from discrete element simulation with friction coefficient $\mu = 0.5$ at $\theta = 0°$ and $\theta = 90°$. The scales in the plots for $\theta = 0°$ and $\theta = 90°$ are identical.

Thornton and Antony (1998) performed three-dimensional discrete element simulations with 8000 spheres. Considering the limited size of their assembly, they (naturally) did not consider the PDF for a fixed contact orientation θ, but instead considered the PDF for the normal forces obtained when all orientations are combined. They found a trend (from initial isotropic state, to state at peak strength and then to large strain) similar to that shown here in Fig. 8.

5. Maximum entropy method

The (naive) definition of entropy I of the PDF $P_f(\boldsymbol{f})$ is $I(P_f) = \int_f -\ln P_f P \,\mathrm{d}\boldsymbol{f}$, implying a single average of the contact forces that is independent of contact orientation θ. However, as shown in Fig. 2, the average contact forces will in general depend significantly on contact orientation θ. Using the notation (6) for overall averages, a proper definition of entropy is therefore given in terms of the conditional PDF $P_f(\boldsymbol{f}|\theta)$

$$I(P_f) = \int_0^{2\pi} S(\theta)\,\mathrm{d}\theta \int_{\boldsymbol{f}} -\ln P_f(\boldsymbol{f}|\theta) P_f(\boldsymbol{f}|\theta)\,\mathrm{d}\boldsymbol{f} = -\langle \ln P_f \rangle \tag{16}$$

This definition of information entropy for quasi-static deformation of granular materials was first proposed by Rothenburg (1980). A detailed motivation of (16) is given by Rothenburg and Kruyt (in preparation) and Kruyt and Rothenburg (2002a). The central assumption made is that forces at contacts with similar orientations θ can be treated as *independent* realisations of a random variable with the conditional PDF $P_f(\boldsymbol{f}|\theta)$. By counting the multitude of all possible responses, it is observed that the most probable outcome is found when this information entropy attains a maximum, like in the numerous applications of information theory (Katz, 1967; Kapur and Kesavan, 1992).

Although the contact forces involving a single particle are not independent, since they satisfy the quasi-static force equilibrium equations for the particles, contacts with similar orientations θ are practically independent (at least for assemblies with sufficient geometrical disorder and small correlation lengths), since such contacts are spatially separated. An analogy with a system consisting of a mixture of gases in kinetic theory is that contacts with similar orientations θ each constitute an independent subsystem.

The maximum entropy method *postulates* that the PDF $P_f(\boldsymbol{f}|\theta)$ is determined by maximizing the entropy (16) under the constraints that apply to the case considered. These constraints form the macroscopic information available about the system. A universal constraint is the normalisation condition (5).

The maximum entropy method will be used here to determine the conditional PDF $P_{\mathrm{nt}}(f_{\mathrm{n}}, f_{\mathrm{t}}|\theta)$ for the normal and tangential forces. Part of the derivation by Kruyt and Rothenburg (2002b) is repeated here to make the current presentation self-contained. The maximization of information entropy will be performed subject to the constraints formed by the given stress tensor (7) and the normalising condition (5) for $P_{\mathrm{nt}}(f_{\mathrm{n}}, f_{\mathrm{t}}|\theta)$. Hence these constraints do not involve the kinematics.

Using the method of Lagrangian multipliers, the PDF that corresponds to maximum information entropy (16) is found to be exponential

$$P_{\mathrm{nt}}(f_{\mathrm{n}}, f_{\mathrm{t}}|\theta) = \frac{1}{Z(\theta)} \mathrm{e}^{-\Lambda_{ij} l_j f_i} = \frac{1}{Z(\theta)} \mathrm{e}^{-[\Lambda_{ij} l_j n_i f_{\mathrm{n}} + \Lambda_{ij} l_j t_i f_{\mathrm{t}}]} \tag{17}$$

where Λ_{ij} and $Z(\theta)$ are the Lagrangian multipliers associated with the stress constraint and the normalising condition, respectively. To simplify the notation, some abbreviations are introduced

$$\lambda_{\mathrm{n}} = \Lambda_{ij} l_j n_i \qquad \lambda_{\mathrm{t}} = \Lambda_{ij} l_j t_i \tag{18}$$

where λ_{n} and λ_{t} will in general depend on contact orientation. Then the PDF $P_{\mathrm{nt}}(f_{\mathrm{n}}, f_{\mathrm{t}})$ can be written as

$$P_{\mathrm{nt}}(f_{\mathrm{n}}, f_{\mathrm{t}}|\theta) = \frac{1}{Z} \mathrm{e}^{-(\lambda_{\mathrm{n}} f_{\mathrm{n}} + \lambda_{\mathrm{t}} f_{\mathrm{t}})} \tag{19}$$

The marginal PDF P_{n} for the normal force and the marginal PDF P_{t} for the tangential force are obtained by integration from P_{nt}

$$\begin{aligned} P_{\mathrm{n}}(f_{\mathrm{n}}) &= \int_{-\mu f_{\mathrm{n}}}^{\mu f_{\mathrm{n}}} P_{\mathrm{nt}}(f_{\mathrm{n}}, f_{\mathrm{t}})\, \mathrm{d}f_{\mathrm{t}} = \frac{1}{Z} \left[\frac{\mathrm{e}^{-(\lambda_{\mathrm{n}} - \mu\lambda_{\mathrm{t}}) f_{\mathrm{n}}} - \mathrm{e}^{-(\lambda_{\mathrm{n}} + \mu\lambda_{\mathrm{t}}) f_{\mathrm{n}}}}{\lambda_{\mathrm{t}}} \right] \\ P_{\mathrm{t}}(f_{\mathrm{t}}) &= \int_{|f_{\mathrm{t}}|/\mu}^{\infty} P_{\mathrm{nt}}(f_{\mathrm{n}}, f_{\mathrm{t}})\, \mathrm{d}f_{\mathrm{n}} = \frac{1}{Z} \frac{\mathrm{e}^{-\lambda_{\mathrm{t}} f_{\mathrm{t}}} \mathrm{e}^{-\lambda_{\mathrm{n}} |f_{\mathrm{t}}|/\mu}}{\lambda_{\mathrm{n}}} \end{aligned} \tag{20}$$

After some algebra it follows from (20) that $\bar{1} = (1/Z)[2\mu/(\lambda_{\mathrm{n}}^2 - \mu^2 \lambda_{\mathrm{t}}^2)]$, and hence the Lagrangian multiplier Z associated with the normalising condition (5) becomes

$$Z = \frac{2\mu}{\lambda_{\mathrm{n}}^2 - \mu^2 \lambda_{\mathrm{t}}^2} \tag{21}$$

while the average normal and tangential force are given by

$$\bar{f}_{\mathrm{n}} = \frac{2\lambda_{\mathrm{n}}}{\lambda_{\mathrm{n}}^2 - \mu^2 \lambda_{\mathrm{t}}^2} \qquad \bar{f}_{\mathrm{t}} = \frac{-2\mu^2 \lambda_{\mathrm{t}}}{\lambda_{\mathrm{n}}^2 - \mu^2 \lambda_{\mathrm{t}}^2} \tag{22}$$

Note that the expression for the average tangential force given by Kruyt and Rothenburg (2002b) contains an error. The expressions (22) for the averages $\bar{f}_{\mathrm{n}}$ and $\bar{f}_{\mathrm{t}}$ in terms of the coefficients λ_{n} and λ_{t} can be inverted to give expressions for λ_{n} and λ_{t} in terms of the averages $\bar{f}_{\mathrm{n}}$ and $\bar{f}_{\mathrm{t}}$

$$\lambda_{\mathrm{n}} = \frac{2\mu^2 \bar{f}_{\mathrm{n}}}{\mu^2 \bar{f}_{\mathrm{n}}^2 - \bar{f}_{\mathrm{t}}^2} \qquad \lambda_{\mathrm{t}} = \frac{-2\bar{f}_{\mathrm{t}}}{\mu^2 \bar{f}_{\mathrm{n}}^2 - \bar{f}_{\mathrm{t}}^2} \tag{23}$$

The PDFs for the nondimensional normal force ξ and for the nondimensional tangential force η become

$$P_\xi(\xi) = \frac{\mathrm{e}^{\frac{-2\xi}{1+\rho}} - \mathrm{e}^{\frac{-2\xi}{1-\rho}}}{\rho} \qquad P_\eta(\eta) = \mathrm{e}^{-2\frac{|\eta| - \rho\eta}{1-\rho^2}} \tag{24}$$

where ξ and η are defined in (13) and ρ is given in (14).

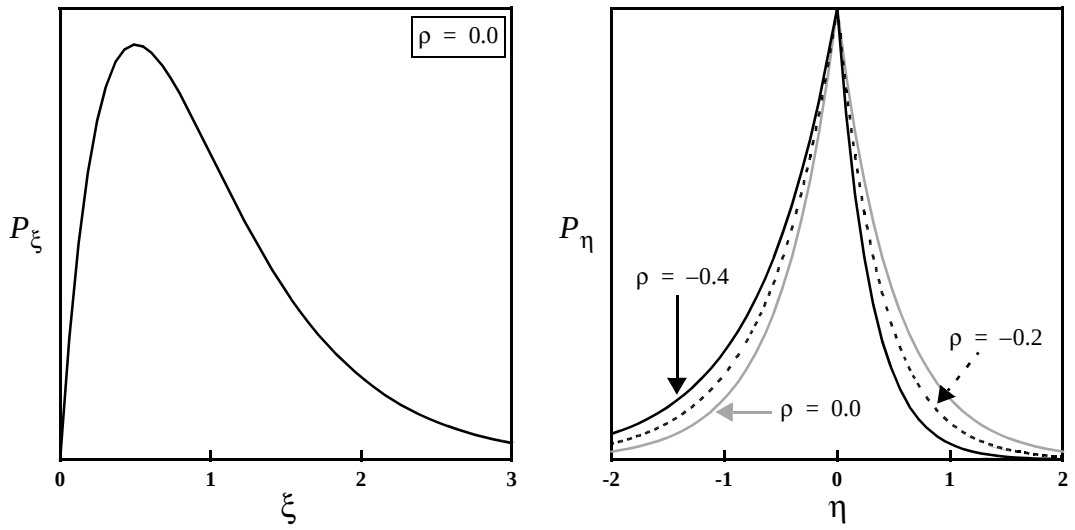

Fig. 12. Theoretical PDF P_ξ for the nondimensional normal force ξ, and theoretical PDF P_η for the nondimensional tangential force η. The latter is shown for various values of the parameter ρ as defined in (14).

These theoretical predictions are shown in Fig. 12. The PDF P_ξ for the nondimensional force ξ is only shown for $\rho = 0$, since the results for other, realistic values of ρ are practically indistinguisable. In fact, from a Taylor expansion it follows that for small ρ and finite ξ and η, we have

$$P_\xi(\xi) = 4\xi e^{-2\xi} + O(\rho^2) \qquad P_\eta(\eta) = e^{-2|\eta|}[1 + 2\rho\eta] + O(\rho^2) \tag{25}$$

Hence the theoretical PDF P_ξ for the normal forces does not depend strongly on friction coefficient. This was also observed experimentally by Blair et al. (2001) and in the discrete element simulations of isotropic assemblies by Kruyt and Rothenburg (2002b). This theoretical PDF P_ξ for the nondimensional force ξ was also obtained by Coppersmith et al. (1996) from a lattice-type model.

The theoretical decay rate r_ξ for the nondimensional normal force is $r_\xi = 2/(1 + |\rho|)$, while the decay rate r_η for the nondimensional tangential force is different for positive and negative tangential forces, i.e. $r_\eta = 2/(1 + \rho)$ for $\eta \gg 1$ and $r_\eta = 2/(1 - \rho)$ for $\eta \ll -1$. The discrete element simulations also show that the decay rates r_η are different for positive and negative η, see Fig. 9.

The PDF P_ξ is qualitatively similar to those observed in the discrete element simulations for the isotropic state and for the anisotropic states for $\theta = 0°$. A difference with the results from the simulations is that the probability density at $\xi = 0$ is underestimated theoretically. The PDF P_ξ for $\theta = 90°$ from the simulations is qualitatively different, since in the simulations the peak of the PDF is found at $\xi = 0$.

The theoretical PDF P_η is qualitatively similar to those observed in the discrete element simulations. It is symmetrical with respect to $\eta = 0$ when $\rho = 0$. When $\rho \neq 0$, the PDF is no longer symmetrical.

5.1. Lagrangian multiplier

Here the Lagrangian multiplier Λ_{ij} associated with the stress constraint (7) will be determined for the case where the particles are disks, the assembly is *anisotropic* with contact density function $S(\theta)$ given by (10) and the stress tensor σ_{ij} in biaxial deformation is

$$\sigma_{ij} = \begin{bmatrix} \frac{1}{2}(p+q) & 0 \\ 0 & \frac{1}{2}(p-q) \end{bmatrix} \tag{26}$$

The corresponding form for the Lagrangian multiplier Λ_{ij} is

$$\Lambda_{ij} = \begin{bmatrix} D(1+E) & 0 \\ 0 & D(1-E) \end{bmatrix} \tag{27}$$

Using (18), (22), (27), $f_i = f_n n_i + f_t t_i$ and $l_i = \bar{l}_n n_i$ for disks, it follows after some lengthy algebra from the stress constraint (26), after linearization in E, that

$$D \cong \frac{m_A}{p} \frac{1+\mu^2-\frac{1}{2}a_c^2}{1+\mu^2-a_c\frac{q}{p}} \qquad E \cong \frac{a_c - 2\frac{q}{p}}{1+\mu^2-a_c\frac{q}{p}} \tag{28}$$

After linearization in a_c and q/p, it follows from (18), (22), (27) and (28) that the Fourier representations of the group averages of the normal and tangential force are

$$\bar{f}_n(\theta) \cong \frac{2p}{m_A \bar{l}_n} + \frac{2p\left(2\frac{q}{p} - a_c\right)}{m_A \bar{l}_n (1+\mu^2)} \cos 2(\theta - \theta_0) \qquad \bar{f}_t(\theta) \cong \frac{-2\mu^2 p\left(2\frac{q}{p} - a_c\right)}{m_A \bar{l}_n (1+\mu^2)} \sin 2(\theta - \theta_0) \tag{29}$$

or for the Fourier components as given in (11)

$$f_0 \cong \frac{2p}{m_A \bar{l}_n} \qquad a_n \cong \frac{2\frac{q}{p} - a_c}{1+\mu^2} \qquad a_t \cong \mu^2 \frac{2\frac{q}{p} - a_c}{1+\mu^2} \tag{30}$$

Note that these results are consistent with the strength–anisotropy–force relation (12). It follows from (30) that according to the maximum entropy method we have

$$\frac{a_t}{a_n} \cong \mu^2 \tag{31}$$

Note that a_t signifies the contribution of the tangential forces to the shear strength q/p, see (11) and (12).

Results from discrete element simulations involving the friction coefficients $\mu = 0.1$, $\mu = 0.3$ and $\mu = 0.5$ are used to study the evolution with shear strain ε_S of the ratio a_t/a_n, see Fig. 13. This ratio gradually decreases until an asymptotic value is attained at larger strains. The values at large strain are compared with the theoretical relation (31) in Fig. 13. It shows that the theoretical value is correct for $\mu = 0.5$, but that it overestimates the ratio a_t/a_n for lower friction coefficients. An accurate fit to the data is obtained by $a_t/a_n = \mu/2$.

Alternatively, one can obtain a relation for a_t by assuming that at some orientation θ, the *average* tangential force is fully mobilised, i.e. $\max_\theta\{|\bar{f}_t(\theta)|/\bar{f}_n(\theta)\} = \mu$. After some algebra it follows that the angle θ^*, at which the maximum is attained, satisfies $\tan 2\theta^* = \sqrt{(1-a_n^2)}/a_n$. Finally, this results in

$$a_t = \mu\sqrt{1-a_n^2} \tag{32}$$

The theoretical values of a_t at large strain are compared to those observed from the discrete element simulations in Table 1. This shows that the values of a_t according to (32), i.e. based on the assumption of fully mobilised average tangential force, greatly overestimate the values of a_t obtained from the results of discrete element simulations.

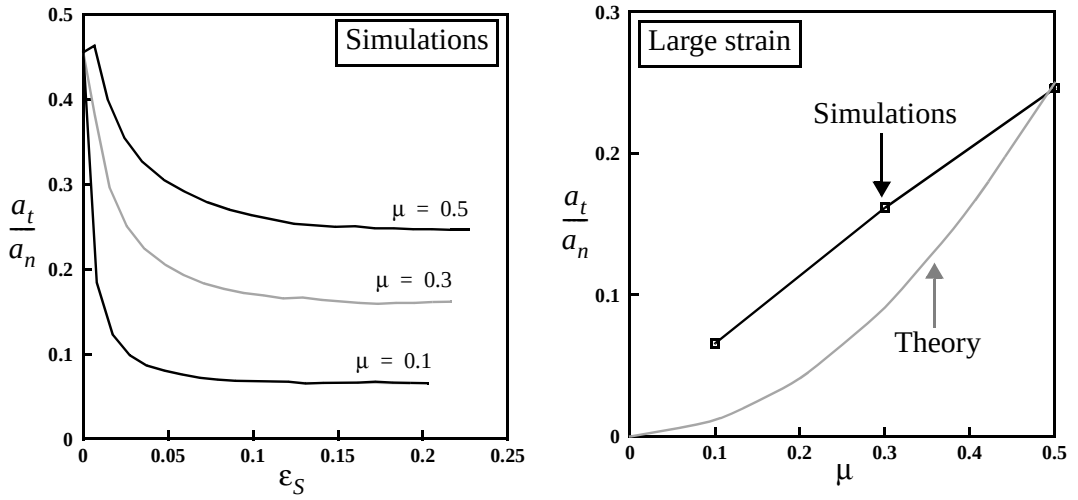

Fig. 13. Evolution of a_t/a_n with shear strain ε_S for various friction coefficients μ from discrete element simulations and comparison of values of a_t/a_n at large strain between results from simulations and the theoretical relation (31).

Table 1
Comparison of theoretical results for a_t with those from discrete element simulations at large strain for various friction coefficients μ

μ	a_t from simulation	a_t from relation (31)	a_t from relation (32)
0.1	0.020	0.003	0.095
0.3	0.061	0.034	0.278
0.5	0.090	0.092	0.465

5.2. Weak contacts

Radjaï et al. (1998) proposed a division of contacts into "strong" contacts with high normal forces and "weak" contacts with low normal forces. From results of computer simulations they observed that the strong contacts and the weak contacts have quite distinct contact density functions. In particular, they noted that the direction of anisotropy of the strong contacts is in the direction of the major principal stress, while that of the weak contacts is in the direction of the minor principal stress. Since we have obtained a theoretical expression for the PDF for the normal forces, it is possible to investigate this division theoretically.

The weak contacts are defined as those contacts at which the normal force is below a threshold, i.e. $f_n^c \leqslant \chi(2p)/(m_A \bar{l}_n)$, where χ is a nondimensional threshold parameter. Note that the factor $(2p)/(m_A \bar{l}_n)$ is equal to the theoretical Fourier coefficient f_0 in (30). Similarly to the contact distribution function $S(\theta)$ of all contacts in the assembly, a contact distribution function $s(\theta;\chi)$ for the weak contacts can be defined by

$$s(\theta;\chi)\,\Delta\theta = \text{Probability}\left(\theta < \theta^c < \theta + \Delta\theta,\ f_n^c \leqslant \chi\frac{2p}{m_A \bar{l}_n}\right) = S(\theta)\,\Delta\theta \int_0^{\chi\frac{2p}{m_A \bar{l}_n}} P_n(f_n|\theta)\,\mathrm{d}f_n \tag{33}$$

where the second equality follows from the definition of conditional probability.

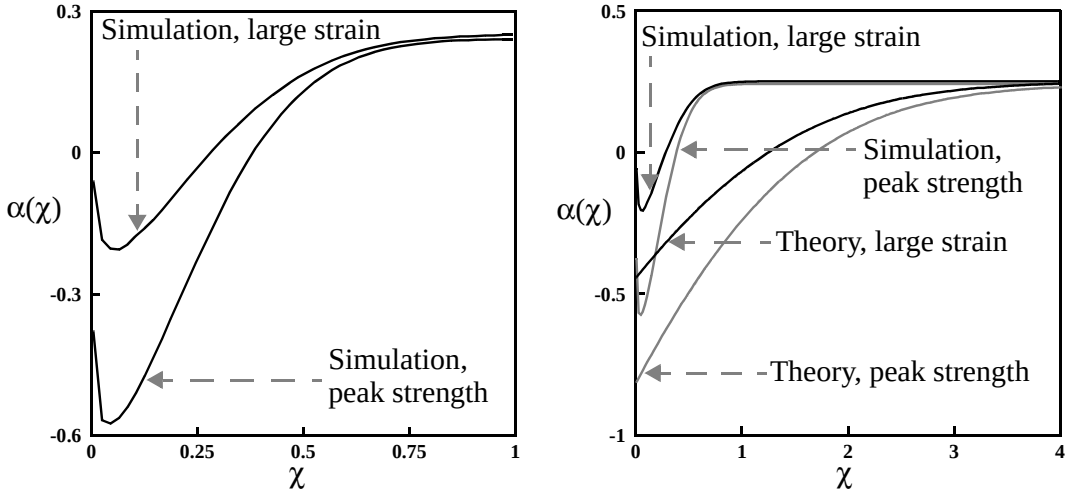

Fig. 14. Anisotropy of "weak" contacts. Results from discrete element simulations with friction coefficient $\mu = 0.5$ at peak strength and at large strain and comparison of theory with results from simulations.

In analogy to (10), the contact distribution function $s(\theta;\chi)$ is represented by a Fourier series

$$s(\theta;\chi) = \frac{1}{2\pi}[1 + \alpha_c(\chi)\cos 2(\theta - \theta_0)] \tag{34}$$

Using a Taylor series expansion in a_c and q/p, it follows after some lengthy algebra from (24), (29) and (33) that the anisotropy $\alpha_c(\chi)$ is given by

$$\frac{a_c - \alpha_c(\chi)}{a_c - \alpha_{c0}} \cong \frac{2\chi^2}{e^{2\chi} - (1 + 2\chi)} \qquad \alpha_{c0} \cong a_c - 2\frac{2\frac{q}{p} - a_c}{1 + \mu^2} \tag{35}$$

Note that $\alpha_{c0} = \alpha_c(\chi \to 0)$ and that $\alpha_c(\chi \to \infty) = a_c$.

The theoretical prediction is compared with results of a discrete element simulation in Fig. 14. The results of the present simulation are in qualitative agreement with those obtained by Radjaï et al. (1998) after noting that their $\langle F \rangle = f_0/(2\pi)$ (see (11)). The theory predicts that the anisotropy becomes negative for small values of χ, which is also observed from the simulations. Note that a negative anisotropy $\alpha(\chi)$ corresponds to the anisotropy of $s(\theta,\chi)$ being in the direction of the minor principal stress. Hence the salient qualitative characteristic of the weak contacts is predicted theoretically. Fig. 14 shows that the theory overestimates the anisotropy at small forces and it underestimates the rate at which the overall anisotropy a_c is approached. This is ultimately related to deviations between the theoretical PDF for the normal forces and the actual PDF observed in the discrete element simulations.

6. Discussion

The PDFs for the contact forces have been studied numerically and theoretically. It is observed that the average forces depend significantly on contact orientation. Therefore the PDFs are also dependent on contact orientation, and it is appropriate to consider the conditional PDFs for the contact forces given the contact orientation. These conditional PDFs are studied numerically, using results from discrete element

simulations of biaxial deformation of a large two-dimensional assembly of 200,000 disks, and theoretically using a maximum entropy method.

As has been observed experimentally, numerically and theoretically for isotropic assemblies, the PDFs also exhibit exponential tails for anisotropic assemblies. For contacts with orientations in the direction of the minor principal stress, the shape of the PDF for the normal forces changes qualitatively from that in the isotropic state. As discussed in Section 4, this difference is caused by the biaxial deformation mechanism, i.e. on the kinematics of deformation. This deformation mechanism results in a reduction of coordination number, i.e. in the disruption of contacts. The contacts that are broken are predominantly oriented in the direction of the minor principle stress. For contact orientations in the principal stress directions the PDFs for the tangential forces retain the same shape in comparison with that in the isotropic state, but they become wider due to the biaxial deformation mechanism which leads to a wider range of tangential forces. For other contact orientations, the PDF for the tangential forces is not symmetrical with respect to zero tangential force. The PDFs for the nondimensional normal and tangential forces are approximately independent of strain beyond the elastic range, except for the PDFs for forces with contact orientations in the direction of the minor principle stress.

The theoretical PDF for the normal forces is qualitatively similar to those observed in the simulations in the isotropic state and in the anisotropic states for contact orientations in the direction of the major principal stress. The major difference between simulations and theory is that the probability of small normal forces is underestimated theoretically. The theoretical PDF for the tangential forces is qualitatively similar to all PDFs observed in the simulations. This includes the asymmetry of the PDF around zero tangential force when the group average tangential force does not equal zero and the different decay rates observed for positive and negative tangential forces.

The maximum entropy theory also results in relation (31) between the components a_t and a_n in the stress–force–fabric relation (12). This relation gives much better agreement with the results of the simulations than relation (32) that is based on the assumption of fully mobilised group average tangential forces. A further salient feature of the theory is that it qualitatively predicts the anisotropy of the weak contacts being in the direction of the minor principle stress.

From experimental studies employing photoelastic materials (for example De Josselin de Jong and Verruijt, 1969; Drescher and de Josselin de Jong, 1972; Oda and Konishi, 1974), it is well-known that *force chains* arise in granular materials, which indicate spatial correlations between contact forces. It is not possible to predict the occurrence of such force chains with the maximum entropy method, since it is assumed in this theory that the contact forces are independent realisations of a random variable, i.e. spatial correlations are absent.

The explanation given in Section 4 for the evolution of the shape of the PDFs is based on considerations of the biaxial deformation mechanism, i.e. on the kinematics. The kinematics are coupled to the statics by the contact constitutive relation (8) that involves the elastic parameters k_n and k_t.

Thornton and Antony (1998) showed on the basis of results of three-dimensional discrete element simulations with fairly small isotropic assemblies that elastic parameters in their contact constitutive relation influence the PDF for the nondimensional normal forces at identical confining hydrostatic stress. Alternatively, they showed that for "soft" particles this PDF depends on the level of confining stress, while for "hard" particles this dependence of this PDF on the stress level is small.

On the basis of dimensional analysis one finds that for two-dimensional isotropic assemblies under hydrostatic confining stress σ and with the contact constitutive relation (8) considered, the PDF for the nondimensional normal forces is given by a functional relation between nondimensional quantities of the form $P_{\xi} = F(\xi, \rho, \mu, \sigma/\{k_n R_{avg}\}, k_t/k_n, \text{PSD})$. Here ρ is given by (14) and PSD denotes the shape of the particle-size distribution. Note that for two-dimensional assemblies the quantity $\sigma/\{k_n R_{avg}\}$ is nondimensional and that the theoretical result (24) is of the form $P_{\xi} = F(\xi, \rho)$. Hence dimensional analysis gives a functional form that contains more nondimensional quantities (such as elastic parameters, confining stress

and particle-size distribution) than the theoretical result (24), but the theoretical analysis yields a specific functional form. The results of Thornton and Antony (1998) demonstrate that the extra nondimensional quantity $\sigma/\{k_n R_{avg}\}$ is important for soft particles (high value of $\sigma/\{k_n R_{avg}\}$), while for hard particles (low value of $\sigma/\{k_n R_{avg}\}$) this quantity has a small influence.

It is recommended to investigate further the effect on the PDFs for the forces of (i) the elastic component of the contact constitutive relation, including the use of more realistic Hertzian-type models, and (ii) the particle-size distribution.

In the present theoretical formulation the kinematics have not been considered. It is expected that a more detailed theoretical description may be obtained by introducing additional constraints involving the *kinematics* into the maximum entropy formulation, for example by prescribing a strain increment. This obviously leads to greatly increased analytical complexity. If this complexity were to be resolved successfully, the resulting theory would give the evolution of the PDF for the contact forces in terms involving a strain increment. Since the stress increment can be determined from the PDF for the contact forces, the result will imply a micromechanical constitutive relation.

Acknowledgement

The author would like to thank L. Rothenburg of University of Waterloo (Waterloo, Canada) for the frequent and very valuable discussions related to this study.

References

Antony, S.J., 2000. Evolution of force distribution in three-dimensional granular media. Physical Review E 63, 011302.

Bagi, K., 1997. Analysis of micro-variables through entropy principle. In: Behringer, R.P., Jenkins, J.T. (Eds.), Powders & Grains '97. Balkema, Rotterdam, The Netherlands, pp. 251–254.

Bathurst, R.J., Rothenburg, L., 1990. Observations on stress–force–fabric relationships in idealized granular materials. Mechanics of Materials 9, 65–80.

Blair, D.L., Mueggenburg, N.W., Marshall, A.H., Jaeger, H.M., Nagel, S.R., 2001. Force distribution in three-dimensional granular assemblies: effects of packing order and interparticle friction. Physical Review E 63, 041304.

Coppersmith, S.N., Liu, C.H., Majumdar, S., Narayan, O., Witten, T.A., 1996. Model for force fluctuations in bead packs. Physical Review E 53, 4673–4685.

Cundall, P.A., 1986. Distinct element methods of rock and soil structure. In: Brown, E.T. (Ed.), Numerical and Analytical Methods in Engineering Rock Mechanics.

Cundall, P.A., Strack, O.D.L., 1979. A discrete numerical model for granular assemblies. Géotechnique 9, 47–65.

De Josselin de Jong, G., Verruijt, A., 1969. Etude photo-élastique d'un empilement de disques. Cahier Groupe Français Rhéologie 2, 73–86.

Drescher, A., de Josselin de Jong, G., 1972. Photoelastic verification of a mechanical model for the flow of a granular material. Journal of the Mechanics and Physics of Solids 20, 337–351.

Horne, M.R., 1965. The behaviour of an assembly of rotound, rigid, cohesionless particles I and II. Proceedings of the Royal Society London A 286, 62–97.

Kapur, J.N., Kesavan, H.K., 1992. Entropy Optimization Principles with Applications. Academic Press, San Diego, CA, USA.

Katz, A., 1967. Principles of Statistical Mechanics: the Information Theory Approach. W.H. Freeman and Company, San Francisco, CA, USA.

Kruyt, N.P., Rothenburg, L., 1996. Micromechanical definition of the strain tensor for granular materials. Journal of Applied Mechanics (Transactions of the ASME) 63, 706–711.

Kruyt, N.P., Rothenburg, L., 2002a. Maximum entropy methods in the mechanics of quasi-static deformation of granular materials. In: Proceedings of International Mechanical Engineering Congress and Exhibition 2002, IMECE02-32494, New Orleans, LA, USA.

Kruyt, N.P., Rothenburg, L., 2002b. Probability density functions of contact forces for cohesionless frictional granular materials. International Journal of Solids and Structures 39, 571–583.

Løvoll, G., Måløy, K.J., Flekkøy, E.G., 1999. Force measurements on static granular materials. Physical Review E 60, 5872–5876.
Makse, H.A., Johnson, D.L., Schwartz, L.M., 2000. Packing of compressible granular materials. Physical Review Letters 84, 4160–4163.
Mehrabadi, M.M., Nemat-Nasser, S., Oda, M., 1982. On the statistical description of stress and fabric in granular materials. International Journal for Numerical and Analytical Methods in Geomechanics 6, 95–108.
Mueth, D.M., Jaeger, H.M., Nagel, S.R., 1998. Force distribution in a granular medium. Physical Review E 57, 3164–3169.
Nguyen, M.L., Coppersmith, S.N., 2000. Scalar model of inhomogeneous elastic and granular media. Physical Review E 62, 5248–5262.
Oda, M., Konishi, J., 1974. Microscopic deformation mechanism of granular material in simple shear. Soils and Foundations 14, 25–38.
Radjaï, F., Jean, M., Moreau, J.J., Roux, S., 1996. Force distributions in dense two-dimensional granular systems. Physical Review Letters 77, 274–277.
Radjaï, F., Wolf, D.E., Jean, M., Moreau, J.J., 1998. Bimodal character of stress transmission in granular packings. Physical Review Letters 80, 61–64.
Rothenburg, L., 1980. Micromechanics of idealised granular materials, PhD Thesis, Department of Civil Engineering, Carleton University, Ottawa, Ontario, Canada.
Rothenburg, L., Bathurst, R.J., 1989. Analytical study of induced anisotropy in idealized granular materials. Géotechnique 39, 601–614.
Rothenburg, L., Kruyt, N.P. Micromechanical definition of an entropy for quasi-static deformation of bonded granular materials, in preparation.
Rothenburg, L., Selvadurai, A.P.S., 1981. A micro-mechanical definition of the Cauchy stress for particulate media. In: Selvadurai, A.P.S. (Ed.), Proceedings of the International Symposium on Mechanical Behaviour of Structured Media, Ottawa, Canada, pp. 469–486.
Socolar, J.E.S., 1998. Average stresses and force fluctuations in noncohesive granular materials. Physical Review E 57, 3204–3215.
Strack, O.D.L., Cundall, P.A., 1978. The distinct element method as a tool for research in granular media: part I. Report National Science Foundation, NSF Grant ENG75-20711.
Thornton, C., 1997. Force transmission in granular media. KONA 15, 81–90.
Thornton, C., Antony, S.J., 1998. Quasi-static deformation of particulate media. Philosophical Transactions of the Royal Society London A 356, 2763–2782.